

1 **On the relationship between continuous measures of canopy**
2 **greenness derived using near-surface remote sensing and satellite-**
3 **derived vegetation products**

4

5 Luke A. Brown^{1*}, Jadunandan Dash¹, Booker O. Ogutu¹ and Andrew D. Richardson²³⁴

6

7 ¹Geography and Environment, University of Southampton, Highfield, Southampton, SO17 1BJ, United
8 Kingdom

9 ²Department of Organismic and Evolutionary Biology, Harvard University, Cambridge, MA 02138, United
10 States

11 ³School of Informatics, Computing and Cyber Systems, Northern Arizona University, Flagstaff, AZ 8601,
12 United States

13 ⁴Center for Ecosystem Science and Society, Northern Arizona University, Flagstaff, AZ 86011, United
14 States

15

16 **Abstract**

17 Over the last two decades, satellite-derived estimates of biophysical variables have been increasingly used
18 in operational services, requiring quantification of their accuracy and uncertainty. Evaluating satellite-
19 derived vegetation products is challenging due to their moderate spatial resolution, the heterogeneity of the
20 terrestrial landscape, and difficulties in adequately characterising spatial and temporal vegetation
21 dynamics. In recent years, near-surface remote sensing has emerged as a potential source of data against
22 which satellite-derived vegetation products can be evaluated. Several studies have focussed on the
23 evaluation of satellite-derived phenological transition dates, however in most cases the shape and
24 magnitude of the underlying time-series are neglected. In this paper, we investigated the relationship
25 between the green chromatic coordinate (GCC) derived using near-surface remote sensing and a range of

26 vegetation products derived from the Medium Resolution Imaging Spectrometer (MERIS) throughout the
27 growing season. Moderate to strong relationships between the GCC and vegetation products derived from
28 MERIS were observed at deciduous forest sites. Weak relationships were observed over evergreen forest
29 sites as a result of their subtle seasonality, which is likely masked by atmospheric, bidirectional reflectance
30 distribution function (BRDF), and shadowing effects. Temporal inconsistencies were attributed to the
31 oblique viewing geometry of the digital cameras and differences in the incorporated spectral bands. In
32 addition, the commonly observed summer decline in GCC values was found to be primarily associated with
33 seasonal variations in brown pigment concentration, and to a lesser extent illumination geometry. At
34 deciduous sites, increased sensitivity to initial increases in canopy greenness was demonstrated by the
35 GCC, making it particularly well-suited to identifying the start of season when compared to satellite-derived
36 vegetation products. Nevertheless, in some cases, the relationship between the GCC and vegetation
37 products derived from MERIS was found to saturate asymptotically. This limits the potential of the approach
38 for the evaluation of the underlying satellite-derived vegetation products, and for the continuous monitoring
39 of vegetation during the growing season, particularly at medium to high biomass study sites.

40

41 **Keywords**

42 Chlorophyll, FAPAR, MERIS, NDVI, PhenoCam, Validation

43

44 *Corresponding author: l.a.brown@soton.ac.uk

45 **1. Introduction**

46 Vegetation is a major component of the biosphere, and the amount and dynamics of vegetation influence
47 a range of biogeochemical processes. Systematic estimates of the biophysical variables that describe
48 vegetation condition are therefore required by the numerical models that enhance our understanding of the
49 environment and climate system (Myneni et al., 2002; Sellers et al., 1997). Such understanding is
50 fundamental to the development of successful environmental policy, and plays a critical role in informing
51 effective climate change mitigation strategy. Estimates of biophysical variables are also essential in the
52 monitoring of forest resources, of which a net loss of 13 million ha per year is estimated to have occurred
53 globally between 2000 and 2010 (FAO, 2010). Similarly, these estimates are highly valuable in the
54 management of agricultural practices, a particularly important consideration in the context of an increasing
55 global population (Foley, et al., 2011; Godfray et al., 2010). As a result, parameters such as the fraction
56 of absorbed photosynthetically active radiation (FAPAR) and leaf area index (LAI) have been designated
57 essential climate variables (ECVs) (GCOS, 2010).

58 The consistent monitoring of vegetation at regional to global scales was first facilitated by the Advanced
59 Very High Resolution Radiometer (AVHRR), which records coarse spectral resolution data at red and near-
60 infrared wavelengths. Over the last two decades, instruments such as the Moderate Resolution Imaging
61 Spectroradiometer (MODIS), Medium Resolution Imaging Spectrometer (MERIS) and Vegetation (VGT)
62 have provided improvements in radiometry, spectral and spatial resolution (Barnes et al., 1998;
63 Maisongrande et al., 2004; Rast et al., 1999). From these data, a range of satellite-derived vegetation
64 products have emerged, providing users with spatially explicit estimates of various biophysical variables.
65 Examples include the CYCLOPES and MOD15 products, which provide estimates of FAPAR and LAI
66 derived from VGT and MODIS respectively (Baret et al., 2007; Myneni et al., 1999), in addition to the MERIS
67 Global Vegetation Index (MGVI), which corresponds to FAPAR (Gobron et al., 1999), and the MERIS
68 Terrestrial Chlorophyll Index (MTCI), a surrogate of canopy chlorophyll content (Dash and Curran, 2004).
69 Over the coming years, the continuity of these products will be ensured by new instruments such as the
70 Ocean and Land Colour Instrument (OLCI), Sea and Land Surface Temperature Radiometer (SLSTR), and
71 Visible Infrared Radiometer Suite (VIIRS) (Donlon et al., 2012; Justice et al., 2013).

72 To be of real use in environmental decision making, it is vital to ensure that satellite-derived vegetation
73 products are of high quality and consistency. This is a particularly important consideration as we enter the
74 era of operational use, in which an increasing number of products will be routinely made available through
75 initiatives such as the European Commission's Copernicus programme (EC, 2005). Scientists, decision
76 makers, and service providers will be provided with an unprecedented volume of data from which to choose,
77 supporting activities such as agricultural monitoring and food security, forest management, numerical
78 weather prediction, and climate modelling. By quantifying the uncertainties associated with satellite-derived
79 vegetation products, their performance can be better understood, enabling users to assess their fitness for
80 purpose and select those data that are most appropriate for their needs (Baret et al., 2005; Justice et al.,
81 2000; Morisette et al., 2002; 2006). The importance of product evaluation is increasingly well recognised,
82 and in recent years initiatives such as the Quality Assurance Framework for Earth Observation (QA4EO)
83 have been established with the endorsement of the Committee on Earth Observation Satellites (CEOS),
84 providing a formal structure for these activities (QA4EO, 2010).

85 Despite its importance, the evaluation of operational satellite-derived vegetation products is particularly
86 challenging as a result of their moderate spatial resolution, which typically ranges from 300 m to 1 km. The
87 in-situ observations that act as reference data are point-based, making direct comparison possible only in
88 areas of high homogeneity (Fernandes et al., 2014; Morisette et al., 2002). Because such homogeneity is
89 uncommon in the terrestrial landscape, particularly at the spatial resolutions of instruments such as MODIS
90 and MERIS, logistically challenging field campaigns are required to adequately characterise spatial
91 variability over a study site. Unfortunately, these activities are constrained by financial resources, reducing
92 their frequency to, at best, a handful of dates per year, thus limiting the extent to which seasonal vegetation
93 dynamics can be characterised.

94 *1.1. The role of near-surface remote sensing*

95 In recent years, near-surface remote sensing has emerged as a potential source of data against which
96 satellite-derived vegetation products can be evaluated, providing potentially valuable information about their
97 performance. Digital cameras provide an inexpensive means by which the greenness of a vegetation
98 canopy can be characterised at a high temporal resolution (Keenan et al., 2014; Richardson et al., 2007;

99 2009; Sonnentag et al., 2012). By making use of the red, green and blue bands of the image, vegetation
100 indices such as the Excess Green Index (EGI) and Green Chromatic Coordinate (GCC) can be calculated,
101 providing a measure of canopy greenness. Importantly, because the field-of-view (FOV) of a digital camera
102 can incorporate an entire canopy, near-surface remote sensing can provide a greater degree of spatial
103 integration than traditional in-situ techniques, better reflecting the moderate spatial resolution of the
104 satellite-derived vegetation products themselves (Hufkens et al., 2012; Keenan et al., 2014; Richardson et
105 al., 2007; 2009).

106 The phenological research community have adopted near-surface remote sensing as an alternative to
107 traditional in-situ observations of events such as bud-burst and leaf opening, which are limited in terms of
108 their spatial extent and species diversity. By analysing time-series of near-surface remote sensing data,
109 phenological transition dates can be determined (Ide and Oguma, 2010; Richardson et al., 2007; 2009;
110 Sonnentag et al., 2012). Recently, near-surface remote sensing has been used in the continuous
111 monitoring of vegetation condition, and has formed the basis of models of plant function (Hufkens et al.,
112 2016; Migliavacca et al., 2011; Toomey et al., 2015). The Phenological Camera (PhenoCam) network is
113 the largest near-surface remote sensing initiative, and is comprised of 340 sites, each equipped with a
114 digital camera that is mounted above or within a vegetation canopy (Richardson et al., 2007; 2009). Of
115 these 340 sites, 230 adhere to a common protocol, whilst 200 record data at both visible and near-infrared
116 wavelengths. Although the majority of PhenoCam sites are located in North America, similar initiatives
117 have more recently been established in other parts of the world (Morra di Cella, 2009; Wingate et al., 2015).

118 Making use of near-surface remote sensing data provided by initiatives such as the PhenoCam network,
119 several studies have focussed on the evaluation of satellite-derived phenological transition dates (Baumann
120 et al., 2017; Coops et al., 2012; Hufkens et al., 2012; Keenan et al., 2014; Klosterman et al., 2014; Nijland
121 et al., 2016). In these studies, it is only the timing of phenological transition dates that is considered in most
122 cases, whilst the shape and magnitude of the underlying time-series are largely neglected. By focusing on
123 phenological transition dates, rates of change, which can be affected by a range of meteorological and
124 biogeochemical factors, are overlooked. Accurately capturing and representing these dynamics is vital for
125 the continuous monitoring of vegetation condition, and for the modelling of plant function. Recently, several

126 authors have observed features in near-surface remote sensing data that appear unrelated to vegetation
127 dynamics, including a spring peak and summer decline (Keenan et al., 2014; Toomey et al., 2015; Yang et
128 al., 2014). Although previous work has attributed the spring peak to the non-linear relationship between
129 leaf chlorophyll concentration and the GCC (Wingate et al., 2015), the factors responsible for the summer
130 decline remain unclear. If the entire time-series is to be successfully made use of, an increased
131 understanding of these discrepancies is required.

132 In this paper, we examine the relationship between continuous measures of canopy greenness derived
133 from PhenoCam data and a range of vegetation products derived from MERIS, an instrument with similar
134 characteristics to OLCI on-board the European Space Agency's (ESA's) recently launched Sentinel-3
135 mission (Donlon et al., 2012; ESA, 2012). In doing so, we hope to answer the following questions:

- 136 • How do continuous measures of canopy greenness derived using near-surface remote sensing relate
137 to satellite-derived vegetation products, and what factors are responsible for observed discrepancies?
- 138 • Can near-surface remote sensing be used as a means to operationally and systematically evaluate
139 these satellite-derived vegetation products?

140 2. Materials and methods

141 2.1. Study sites

142 14 study sites were selected based on the availability of at least 1 year of near-surface remote sensing data
143 within the time period that MERIS was operational (17/05/2002 to 08/04/2012). Only Type 1 PhenoCam
144 sites were considered, as at these sites a standard installation protocol is adhered to, using a single digital
145 camera model (NetCam SC IR, StarDot Technologies). The study sites meeting these criteria were
146 dominated by deciduous forest, but also incorporated evergreen forest and grassland vegetation. All study
147 sites were located within the United States, lying at a low or moderate elevation (Table 1). With the
148 exception of Vaira Ranch and Wind River, which experience a mediterranean climate, all study sites were
149 characterised by a temperate climate.

150 Table 1: Selected study sites and their characteristics.

Study site	Latitude	Longitude	Elevation (m)	Dominant land cover
Arbutus Lake	43.9821	-74.2332	535	Deciduous forest
Bartlett Experimental Forest (IR)	44.0646	-71.2881	268	Deciduous forest
Cary Institute of Ecosystem Studies	41.7839	-73.7341	127	Deciduous forest
Coweeta Hydrologic Laboratory	35.0596	-83.4280	680	Deciduous forest
Harvard Forest	42.5378	-72.1715	340	Deciduous forest
Harvard Forest Hemlock	42.5394	-72.1780	355	Deciduous forest
Little Prospect Hill	42.5420	-72.1850	380	Deciduous forest
Howland Experimental Forest	45.2041	-68.7403	80	Evergreen forest
Hubbard Brook Experimental Forest	43.9439	-71.7019	253	Deciduous forest
Morgan Monroe State Forest	39.3231	-86.4131	275	Deciduous forest
Proctor Maple Research Center	44.5250	-72.8660	403	Deciduous forest
University of Michigan Biological Station	45.5598	-84.7138	230	Deciduous forest
Vaira Ranch	38.4133	-120.9506	129	Grassland
Wind River Experimental Forest	45.8213	-121.9521	371	Evergreen forest

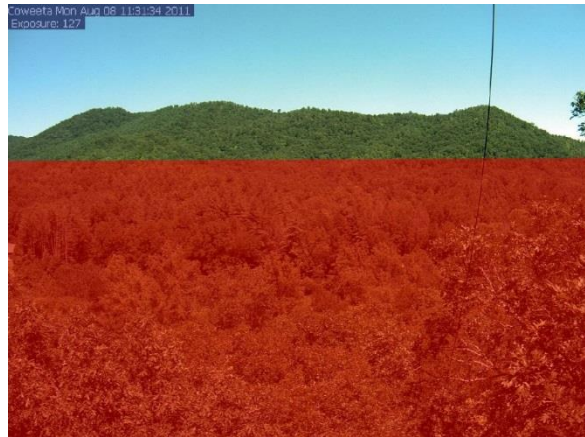
151
152 2.2. Near-surface remote sensing data

153 At each study site, near-surface remote sensing data were obtained from the PhenoCam network. Images
154 acquired between the start of PhenoCam operations and the end of the MERIS archive were selected. At
155 the investigated study sites, images are acquired during daylight hours every 30 minutes. To minimise
156 shadowing and bidirectional reflectance distribution function (BRDF) effects caused by variations in
157 illumination geometry, only near-noon images acquired between the hours of 11:00 and 13:00 local time
158 were considered, providing, on average, 6 images per day (Migliavacca et al., 2011; Richardson et al.,
159 2009). Because the FOV of the digital camera often contained non-canopy features, analysis was restricted

160 to manually defined regions of interest (ROIs) incorporating only the vegetation canopy of interest (Figure
161 1). To minimise the effects of atmospheric aerosols and low-lying cloud, ROIs were restricted to the
162 foreground of the image (Richardson, 2009). For each ROI, the GCC was then calculated as

$$GCC = \frac{DN_{green}}{DN_{red} + DN_{green} + DN_{blue}} \quad (1)$$

163
164 where DN_{green} , DN_{red} and DN_{blue} are mean digital number (DN) values in the green, red and blue bands of
165 the image. The GCC is widely used as a measure of canopy greenness, and when compared to alternatives
166 such as the EGI, it is thought to be more effective at suppressing the effects of variations in scene illumination
167 (Richardson et al., 2007; Sonnentag et al. 2012). As very few sites were acquiring near-infrared data before
168 the end of the MERIS archive, near-infrared capabilities were not investigated in this study.



169
170
171 Figure 1: Example of an ROI incorporating only the vegetation canopy of interest at Coweeta Hydrologic Laboratory
172 (red).
173

174 Because of the comparatively short atmospheric path associated with near-surface remote sensing data,
175 they are typically subject to minimal atmospheric effects when compared with satellite remote sensing data.
176 Nevertheless, noise may be introduced by external conditions such as rain, fog, and condensation, in
177 addition to variations in scene illumination. To suppress such noise, the moving window approach described
178 by Sonnentag et al. (2012) was adopted, in which the 90th percentile of all GCC values acquired within a 3
179 day window was assigned to the central day. To eliminate residual noise, a simple outlier removal

180 procedure was adopted, in which GCC values lying further than 2 standard deviations from the mean of the
181 time-series were excluded from further analysis.

182 *2.3. Satellite remote sensing data*

183 MERIS level 2 full-resolution full-swath (MER_FRS_2P) data were obtained for a 3 x 3 window (900 m x
184 900 m) centred on the location of each study site. Over land surfaces, MER_FRS_2P data incorporate two
185 operational vegetation products: the MGVI and MTCI, in addition to bottom-of-atmosphere (BOA)
186 reflectance values in 13 spectral bands. These BOA reflectance values are the result of a partial
187 atmospheric correction for gaseous absorption and Rayleigh scattering (Santer et al., 2010). The 3 x 3
188 window was selected to minimise uncertainties associated with positional errors and the instrument's point
189 spread function. For each acquisition, the mean value of each measurement data set (MDS) within the
190 window was calculated, except where cloud or relevant product confidence flags were present. These
191 initial data processing steps were carried out remotely using ESA's Grid Processing on Demand (G-POD)
192 environment. By making use of computing resources close to the MERIS archive itself, we could overcome
193 the challenges associated with processing such a large number of acquisitions.

194 Further data processing was carried out locally using a series of Interactive Data Language (IDL) routines.
195 As a result of known deficiencies in the MERIS cloud-screening algorithm (Gomez-Chova et al., 2007; ESA,
196 2006), an additional means of quality control was adopted. Because large variations within the 3 x 3 window
197 were only likely under conditions such as partial cloud cover, the coefficient of variation was calculated, and
198 only acquisitions with a coefficient of variation of < 0.50 were retained for further analysis. Such an approach
199 has been previously applied to MERIS data acquired over the marine environment using an arbitrarily
200 determined coefficient of variation of between 0.15 and 0.25 (Barker et al., 2008; Sá et al., 2015; Mélin et
201 al., 2011). As a greater degree of heterogeneity is likely to be experienced over the terrestrial environment,
202 we selected an increased coefficient of variation for the purposes of this study.

203 Two operational vegetation products were examined: the MGVI and the MTCI. In addition to these
204 products, two alternative vegetation indices were calculated. The Normalised Difference Vegetation Index
205 (NDVI), which demonstrates strong relationships with FAPAR and LAI, was selected as a result of its
206 widespread use (Carlson and Ripley, 1997; Myneni and Williams, 1994; Rouse et al., 1973), whilst the

207 MERIS GCC (hereafter referred to as the MGCC) was selected to provide a more direct spectral comparison
208 to the GCC derived using near-surface remote sensing data. The NDVI was calculated as

$$NDVI = \frac{R_{band\ 13} - R_{band\ 8}}{R_{band\ 13} + R_{band\ 8}} \quad (2)$$

209
210 where $R_{band\ 13}$ and $R_{band\ 8}$ are reflectance values in MERIS bands 13 and 8, centered at 865 nm and 681.25
211 nm respectively, whilst the MGCC was calculated as

$$MGCC = \frac{R_{band\ 5}}{R_{band\ 2} + R_{band\ 5} + R_{band\ 8}} \quad (3)$$

212
213 where $R_{band\ 2}$ and $R_{band\ 5}$ are reflectance values in MERIS bands 2 and 5, centered at 442.5 nm and 560
214 nm respectively. Once calculated, the outlier removal procedure described in Section 2.2 was again
215 adopted to eliminate residual noise.

216 *2.4. Analysis of paired data*

217 MERIS acquisitions were paired to the GCC value representing the 3 day time period within which they fell.
218 To enable the agreement of the two data sets to be assessed, time-series of the GCC and each satellite-
219 derived vegetation product were plotted for each study site. As the data from most study sites demonstrated
220 a strong two-phase seasonal pattern, measures of linear correlation were ill-suited to characterising these
221 relationships. We therefore adopted the non-parametric Spearman's rank correlation coefficient, providing
222 a means to quantify the strength of monotonic relationships between the two variables. To investigate
223 seasonal variations in these relationships, analysis was also carried out on spring, summer, autumn and
224 winter subsets, which were defined according to meteorological definitions for the northern hemisphere.

225 *2.5. Land cover data*

226 To support interpretation of the results, high spatial resolution (30 m) land cover data were obtained from
227 the 2011 National Land Cover Database (NLCD 2011), which consists of 20 land cover classes covering 8
228 broad categories (Homer et al., 2015) (Table 2). To enable the effects of land cover heterogeneity and the

229 influence of different land cover mixtures to be assessed, the percentage of each land cover class was
 230 calculated for a 31 x 31 (930 m x 930 m) window centred on the location of each study site.

231 Table 2: Classification system adopted by the NLCD 2011 (Homer et al., 2015).

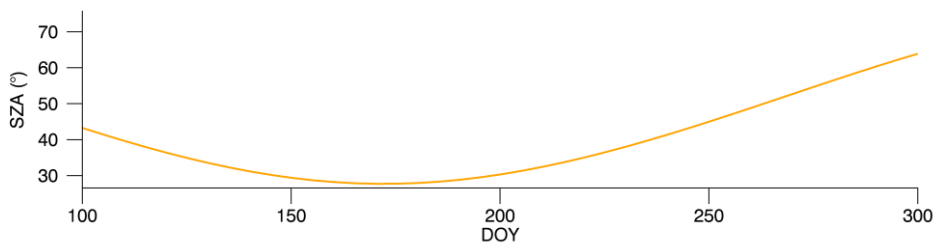
Category	Classes
Water	Open water Perennial ice/snow
Developed	Developed (open space) Developed (low intensity) Developed (medium intensity) Developed (high intensity)
Barren	Barren land (rock/sand/clay)
Forest	Deciduous forest Evergreen forest Mixed forest
Shrubland	Dwarf scrub Shrub/scrub
Herbaceous	Grassland/herbaceous Sedge/herbaceous Lichens Moss
Planted/cultivated	Pasture/hay Cultivated crops
Wetlands	Woody wetlands Emergent herbaceous wetlands

232

233 2.6 Radiative transfer modelling

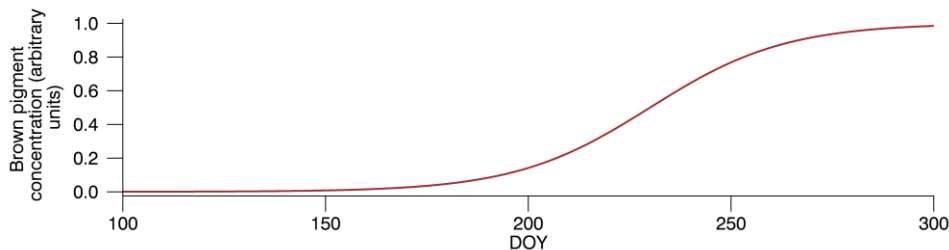
234 To explore factors that could be responsible for the previously observed summer decline, several
 235 experiments were carried out using the Leaf Optical Properties Spectra (PROSPECT) and Scattering by
 236 Arbitrarily Inclined Leaved (SAIL) radiative transfer models (Jacquemoud and Baret 1990; Jacquemoud et
 237 al., 2009; Verhoef, 1984). Coupled, these models provide a physically-based means of investigating how
 238 the combined interaction of various biophysical and non-canopy variables might influence the GCC, and
 239 are particularly useful given the absence of appropriate and contemporaneous ancillary data. To this end,
 240 we extended the analysis of Wingate et al. (2015), who simulated GCC values over the course of a year,
 241 making use of input parameters that reflect empirical observations at the oak-dominated Alice Holt
 242 Research Forest in Southern England (Appendix A). The site is representative of temperate deciduous
 243 forest, having similar characteristics to many of the deciduous forest sites investigated in this study. To

244 investigate whether variations in illumination geometry could contribute to the summer decline, we
245 simulated the GCC using both a fixed solar zenith angle (SZA) of 30°, and a varying SZA calculated at noon
246 for each day of year (DOY) (Figure 2). We also carried out simulations using an alternative parameterisation
247 of brown pigment concentration (Figure 3), as although Wingate et al. (2015) note that the GCC is sensitive
248 to this variable, their parameterisation poorly reflects seasonal variations typically observed in oak, with
249 increases beginning to occur only at DOY 275. In contrast, previous research has demonstrated that
250 increases in the concentration of brown pigments such as tannins instead begin to occur as early as DOY
251 150 (Feeny and Bostock, 1968).



252
253
254

Figure 2: Noon SZA at Alice Holt Research Forest for each DOY simulated.



255
256
257

Figure 3: Alternative brown pigment concentration parameterisation adopted to better reflect seasonal variations typically observed in oak, after Feeny and Bostock (1968).

258 **3. Results**

259 *3.1. Seasonal patterns in the GCC and vegetation products derived from MERIS*

260 Clear seasonal patterns were observed in the GCC at the majority of study sites investigated. They were
261 best resolved at deciduous forest sites, in which the start of the growing season occurred between April
262 and May and the end of the growing season occurred between October and November, depending on the
263 study site. These seasonal patterns were broadly consistent with those observed in the vegetation products
264 derived from MERIS, with the exception of the MGCC, which was subject to a substantial degree of noise
265 (Figure 4). At evergreen forest sites such as Howland Experimental Forest, and Wind River, the GCC was
266 subject to a greater degree of noise (Figure 5). Despite this, seasonal patterns were more clearly resolved
267 by GCC than by the vegetation products derived from MERIS. Similar results were also observed at Vaira
268 Ranch, a grassland site.

269 Although similar temporal patterns were observed between vegetation products derived from MERIS and
270 GCC, they were subject to substantial differences in timing. At the start of the growing season, increases
271 in the GCC occurred by up to 1 month prior to those in the vegetation products derived from MERIS.
272 Conversely, at the end of the growing season, decreases in the vegetation products derived from MERIS
273 occurred by up to 1 month earlier to those in the GCC. Thus, the length of the growing season observed
274 in the vegetation products derived from MERIS was substantially shorter than in the GCC. These
275 differences in timing were most pronounced in the case of the MGVI and MTCl (Figure 4). Additionally, at
276 the majority of deciduous forest sites, an asymmetric pattern was observed, in which peak GCC values
277 occurred in late spring, before an intermediate state of more gradual decline throughout the summer (Figure
278 4). This pattern was observed on an annual basis, but was not evident in the vegetation products derived
279 from MERIS, in which peak values occurred later in the growing season.

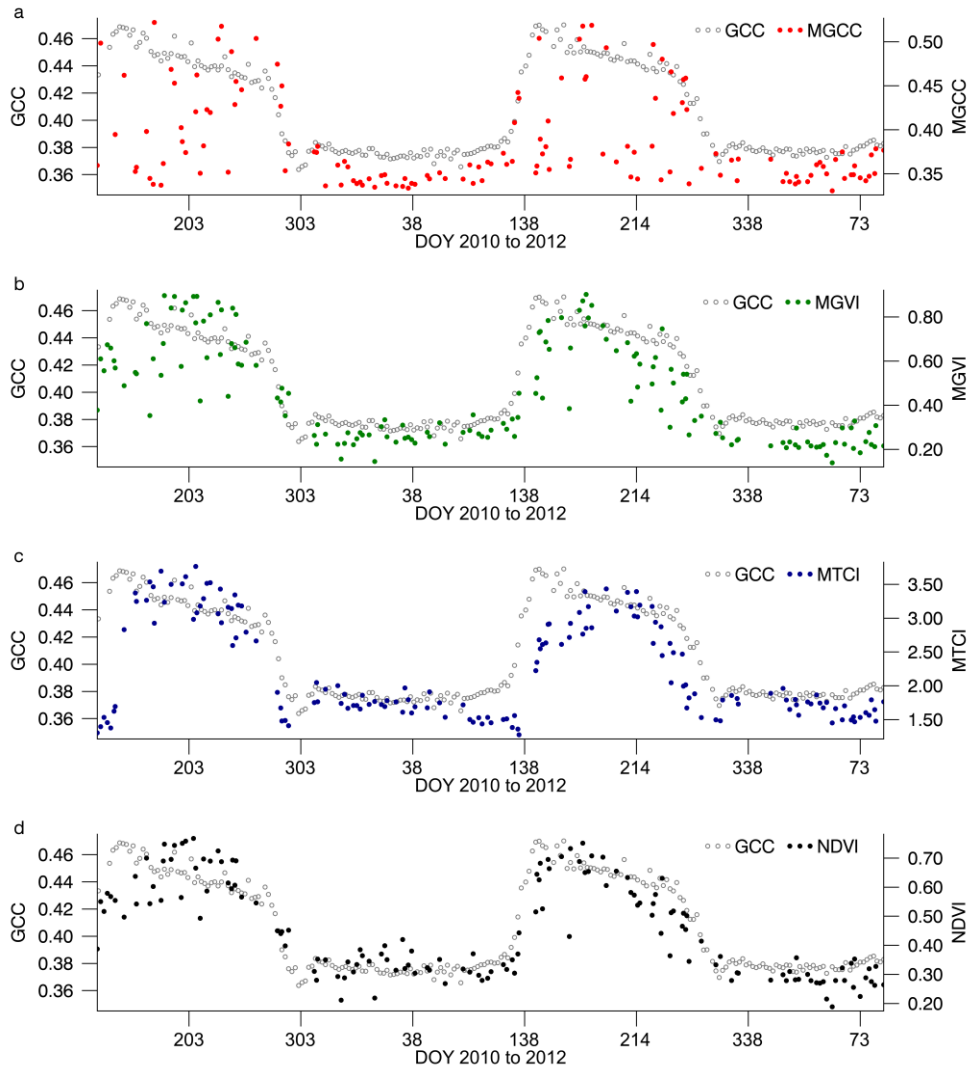


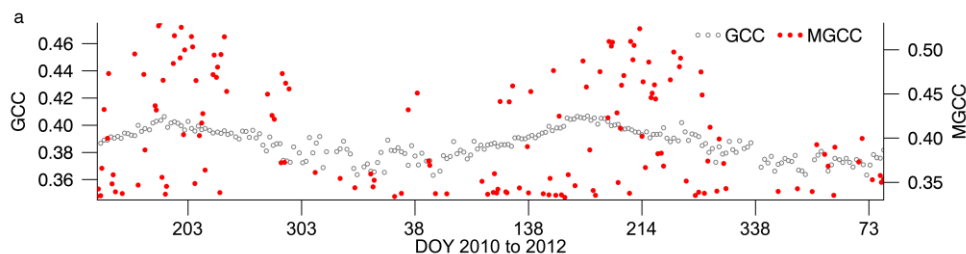
Figure 4: Seasonal patterns in the GCC and MGCC (a), MGVI (b), MTCI (c), and NDVI (d) at Harvard Forest, a deciduous forest site.

3.2. Relationships between the GCC and vegetation products derived from MERIS

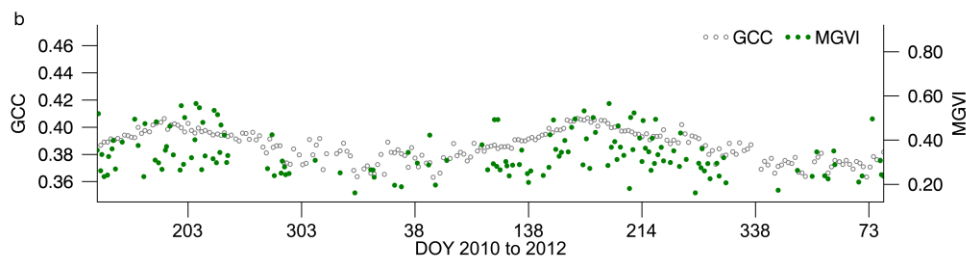
A substantial degree of variability was observed in the strength of the relationships between the GCC and each vegetation product derived from MERIS (Table 3). Moderate relationships were demonstrated by the MGVI, MTCI, and NDVI. In contrast, comparatively weak relationships were demonstrated by the MGCC. The relationships between the GCC and vegetation products derived from MERIS were also subject to a substantial degree of variability between study sites (Table 3). Moderate to strong relationships were demonstrated at study sites dominated by deciduous forest, with the exception of Hubbard Brook Experimental Forest, at which weaker relationships were demonstrated. At some study sites in which

295 several juxtaposing land cover types dominated, such as Cary Institute of Ecosystem Studies, weaker
 296 relationships were too observed. However, this was not the case at others, such as Harvard Forest,
 297 Harvard Forest Hemlock, and Little Prospect Hill. Particularly weak relationships were demonstrated at
 298 study sites dominated by evergreen forest, such as Howland Experimental Forest and Wind River. Similarly
 299 weak relationships were observed at Vaira Ranch, a grassland site. In terms of seasonal differences,
 300 significant relationships between the GCC and vegetation products derived from MERIS were observed at
 301 10 study sites during spring and 13 study sites during autumn. In contrast, significant relationships were
 302 observed at only 1 study site during the summer and 2 study sites during the winter (Appendix B).

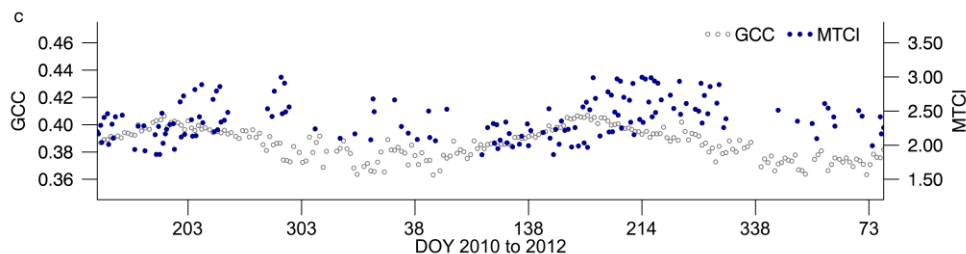
303



304



305



306
 307
 308

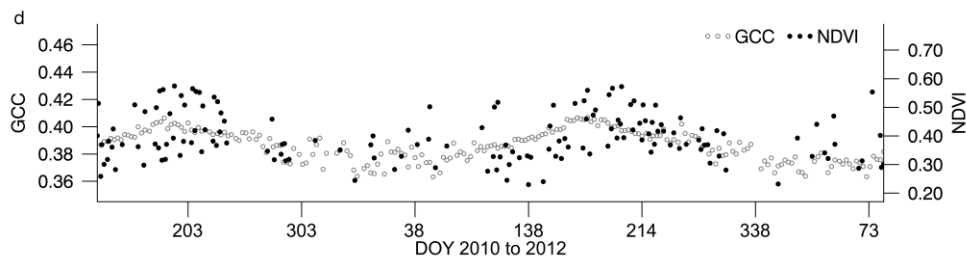


Figure 5: Seasonal patterns in the GCC and MGCC (a), MGVI (b), MTCI (c), and NDVI (d) at Wind River, an evergreen forest site.

309
310
311

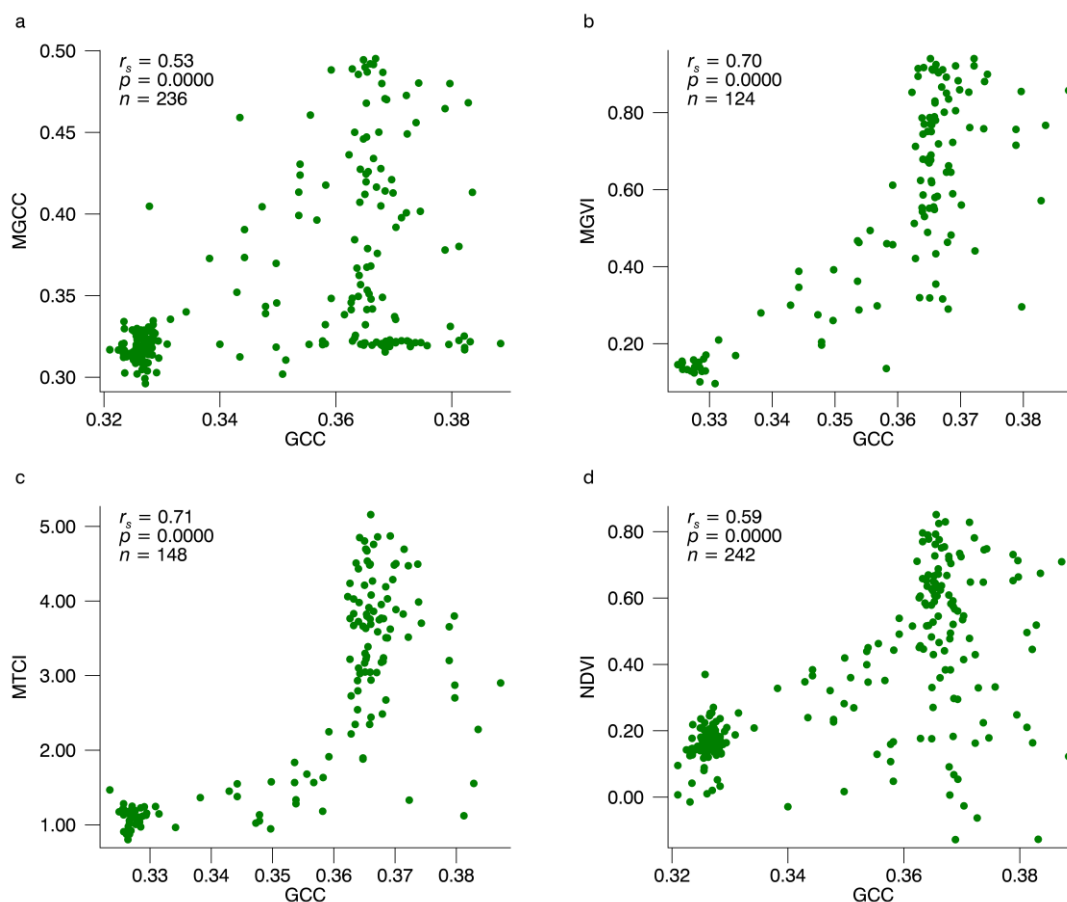
Table 3: Spearman's rank correlation coefficient (r_s) values associated with each satellite-derived vegetation product at each study site. Values marked with * indicate that the relationship with the GCC was statistically significant ($p < 0.01$). For clarity, only land cover classes accounting for $> 1\%$ are shown.

Study site	Land cover classes (%)	MGCC	MGVI	MTCI	NDVI
Arbutus Lake	Deciduous forest (79.9)	0.59*	0.70*	0.55*	0.72*
	Open water (7.8)				
	Evergreen forest (6.3)				
	Mixed forest (4.1)				
	Developed open (1.9)				
Bartlett Experimental Forest (IR)	Deciduous forest (59.0)	0.33*	0.78*	0.58*	0.41*
	Mixed forest (36.4)				
	Shrub/scrub (2.0)				
	Developed open (1.7)				
Cary Institute of Ecosystem Studies	Deciduous forest (44.3)	0.35*	0.53*	0.58*	0.44*
	Pasture/hay (16.4)				
	Evergreen forest (14.8)				
	Developed open (9.5)				
	Shrub/scrub (4.7)				
	Developed low (3.6)				
	Mixed forest (3.6)				
Woody wetlands (2.7)					
Coweeta Hydrologic Laboratory	Deciduous forest (80.6)	0.39*	0.75*	0.80*	0.76*
	Developed open (12.5)				
	Pasture/hay (2.7)				
	Evergreen forest (1.7)				
	Shrub/scrub (1.7)				
Harvard Forest	Deciduous forest (46.2)	0.58*	0.78*	0.64*	0.77*
	Evergreen forest (18.7)				
	Woody wetlands (14.9)				
	Mixed forest (14.2)				
	Developed open (4.4)				
	Shrub/scrub (1.7)				
Harvard Forest Hemlock	Deciduous forest (45.5)	0.55*	0.76*	0.63*	0.73*
	Evergreen forest (26.5)				
	Woody wetlands (24.9)				
	Mixed forest (2.6)				
Little Prospect Hill	Deciduous forest (43.8)	0.65*	0.86*	0.76*	0.85*
	Mixed forest (25.2)				
	Evergreen forest (18.1)				
	Developed open (7.5)				
	Woody wetlands (5.4)				
Howland Experimental Forest	Evergreen forest (90.8)	0.42*	0.54*	0.35*	0.50*
	Woody wetlands (5.1)				
	Mixed forest (4.0)				
Hubbard Brook Experimental Forest	Deciduous forest (54.8)	0.40*	0.57*	0.48*	0.35*
	Mixed forest (31.7)				
	Evergreen forest (6.7)				
	Developed open (3.3)				
	Cultivated crops (2.0)				
Morgan Monroe State Forest	Deciduous forest (92.4)	0.53*	0.70*	0.71*	0.59*
	Shrub/scrub (7.6)				
Proctor Maple Research Center	Deciduous forest (95.8)	0.67*	0.73*	0.62*	0.79*
	Evergreen forest (1.8)				
	Woody wetlands (2.4)				
University of Michigan Biological Station	Deciduous forest (85.38)	0.40*	0.70*	0.81*	0.78*
	Mixed forest (5.2)				
	Grassland/herbaceous (4.3)				
	Developed open (2.0)				
	Evergreen forest (1.4)				
Vaira Ranch	Grassland/herbaceous (79.0)	-0.56*	-0.71*	0.48*	-0.71*
	Deciduous forest (11.7)				
	Developed open (6.7)				
	Shrub/scrub (2.6)				
Wind River Experimental Forest	Evergreen forest (89.2)	0.26*	0.50*	-0.08	0.41*
	Woody wetlands (6.0)				
	Developed low (3.1)				
	Shrub/scrub (1.4)				

312

313 3.3. Characteristics of the GCC

314 Although the range of the vegetation products derived from MERIS was relatively consistent between study
315 sites, a greater degree of variability was observed in the range of GCC values. Additionally, the
316 relationships between the GCC and vegetation products derived from MERIS demonstrated distinct non-
317 linearity at some study sites, taking an exponential form (Figure 6). The GCC was observed to saturate
318 asymptotically at medium to high MGCC, MGVI, MTCI, and NDVI values, whilst demonstrating increased
319 sensitivity to low levels of canopy greenness when compared to these satellite-derived vegetation products.
320 These saturation effects were most pronounced at Morgan Monroe State Forest and Little Prospect Hill.



321

322

323

324

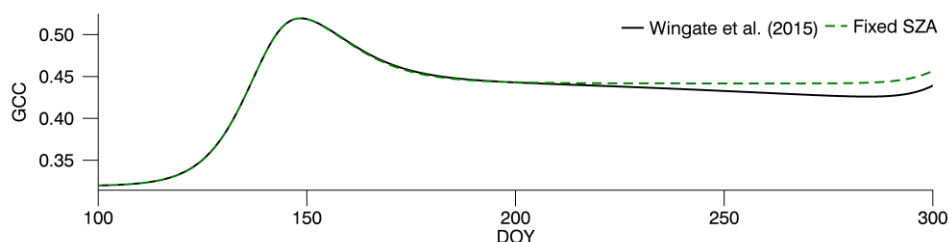
325

Figure 6: Relationships between the GCC and MGCC (a), MGVI (b), MTCI (c), and NDVI (d) at Morgan Monroe State Forest, where r_s is the Spearman's rank correlation coefficient, p is the two-tailed p -value and n is the number of data points.

326

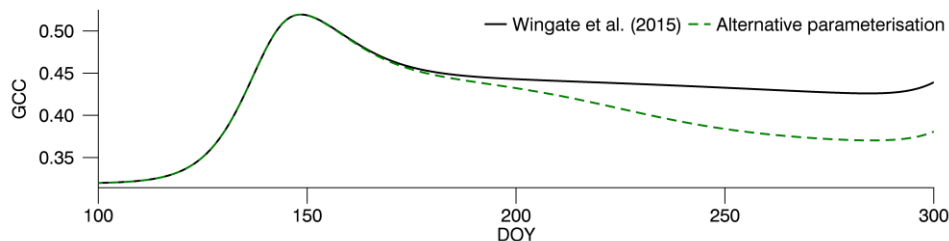
327 3.4. Factors responsible for the summer decline

328 The GCC values simulated using input parameters reflecting empirical observations at Alice Holt Research
329 Forest appear broadly consistent with those observed at other deciduous forest sites, taking on a similar
330 range and seasonal pattern (Figure 7). These simulated values are characterised by an evident spring
331 peak, although a clear summer decline is not observed when a fixed SZA is adopted (Figure 7). A distinct
332 decline is observed throughout the summer months when a varying SZA is adopted as in Wingate et al.
333 (2015), although this decline is of a relatively small magnitude compared to that observed at other
334 deciduous forest sites investigated in this study (Figure 7). When run with our alternative parameterisation
335 of brown pigment concentration, the magnitude of the decline in simulated GCC values is greatly increased,
336 better reflecting observations over these deciduous forest sites (Figure 8).



337 Figure 7: GCC values simulated using a fixed SZA of 30°, in addition to varying SZA as in Wingate et al. (2015).
338

339



340 Figure 8: GCC values simulated using the brown pigment concentration parameterisation based on that of Wingate et
341 al. (2015), in addition to those simulated using our alternative parameterisation (Figure 3).
342

343 4. Discussion

344 4.1. Differences in seasonal patterns observed in the GCC and satellite-derived vegetation products

345 The temporal inconsistencies observed between the GCC and vegetation products derived from MERIS at
346 the start of the growing season are consistent with the results of previous studies. Similar results have
347 been reported when the GCC has been compared with estimates of gross primary productivity (GPP)
348 derived from eddy covariance data, in addition to a range of biophysical variables observed at both the leaf
349 and canopy scale (Keenan et al., 2014; Toomey et al., 2015; Yang et al., 2014). It is suggested by Keenan
350 et al. (2014) that due to the oblique angle at which the digital cameras are mounted, the effective LAI
351 incorporated within their FOV is greater than that observed from a near-nadir viewing geometry, from which
352 only the tops of trees are visible. Changes in canopy greenness are therefore accentuated at the start of
353 the growing season, leading to a more rapid increase in the GCC. In addition to differences in viewing
354 geometry, temporal inconsistencies are also to be expected because of differences in the incorporated
355 spectral bands, which provide sensitivity to different biophysical variables. These biophysical variables
356 have independent but related seasonal trajectories (Yang et al., 2014).

357 The spring peak and summer decline observed at deciduous forest sites (Figure 4) have both been noted
358 in previous work (Keenan et al., 2014; Toomey et al., 2015; Yang et al., 2014), and a number of explanations
359 have been proposed in the literature. For example, using a series of radiative transfer model experiments,
360 Wingate et al. (2015) attribute the spring peak to the non-linear relationship between leaf chlorophyll
361 concentration and the GCC. In early spring, increases in leaf chlorophyll concentration are initially met with
362 increases in the GCC. Peak GCC values are reached at a leaf chlorophyll concentration of approximately
363 $30 \mu\text{g cm}^{-2}$ during late spring, and with further increases in leaf chlorophyll concentration, a reduction in the
364 GCC is observed. We suggest the reason for this reduction is the broadening of the chlorophyll absorption
365 feature, which acts to reduce reflectance at green wavelengths (Gates et al., 1965; Lichtenthaler et al.,
366 1998; Richardson et al., 2002). In terms of the summer decline, several authors have pointed to the role
367 of leaf ageing and associated changes in pigmentation (Keenan et al., 2014; Sonnentag et al., 2012).
368 Despite this, previous work has demonstrated that at deciduous forest sites, leaf chlorophyll concentration
369 remains relatively constant throughout the growing season, and pronounced asymmetry is rarely observed

370 (Gond et al., 1999; Demarez et al., 1999; Koike et al., 1990; Yang et al., 2014). The results of our radiative
371 transfer modelling suggest that seasonal variations in brown pigment concentration are the major
372 contributor to the summer decline, whilst other factors, such as seasonal variations in illumination geometry,
373 also play a minor role.

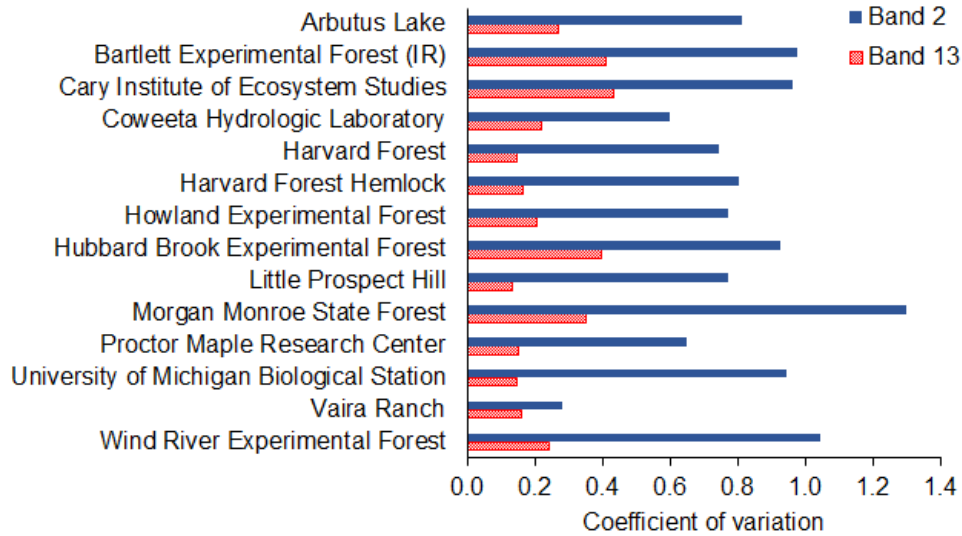
374 *4.2. Differences in relationships between the GCC and satellite-derived vegetation products*

375 The moderate to strong relationships demonstrated between the GCC and MGVI, MTCI, and NDVI at
376 deciduous forest sites reflect the results of previous studies. For example, moderate to strong relationships
377 between the GCC and estimates of GPP derived from eddy covariance data ($r^2 = 0.50$ to 0.82) are
378 presented by Toomey et al. (2015). At evergreen forest sites, weaker relationships are demonstrated as a
379 result of the comparatively subtle seasonality of these species, which was poorly resolved by vegetation
380 products derived from MERIS. It is likely that this relatively weak signal is masked by atmospheric, BRDF,
381 and shadowing effects in the satellite-derived vegetation products, leading to substantial variability within
382 the growing season that is unrelated to vegetation dynamics. Because these effects are less pronounced
383 in the near-surface remote sensing data, this weak signal can be more easily resolved by the GCC. This
384 result indicates that if MERIS and future OLCI data are to prove useful in monitoring evergreen forest sites,
385 more rigorous atmospheric and BRDF correction schemes will be required. The weak relationships
386 demonstrated at Vaira Ranch differ from those presented in previous studies, in which clear seasonal
387 patterns are observed (Liu et al., 2017). In previous work over grassland sites, strong relationships between
388 the GCC and vegetation indices derived from in-situ spectroradiometric observations have been reported
389 ($r^2 = 0.69$ to 0.82), as have strong relationships between the GCC and estimates of GPP derived from eddy
390 covariance data ($r^2 = 0.55$ to 0.92) (Migliavacca et al., 2011; Toomey et al., 2015). This result should
391 therefore be treated with caution, particularly in light of the fact that only a single grassland site was
392 investigated.

393 When comparing phenological transition dates derived from PhenoCam data and vegetation products
394 derived from MODIS, Klosterman et al. (2014) report a strong relationship between fractional forest cover
395 and bias in the end of spring date ($r^2 = 0.73$). Nevertheless, significant relationships ($p < 0.05$) were not
396 reported for any other investigated phenological transition dates. Similarly, in this study, observed patterns

397 between land cover heterogeneity and the strength of the relationships between the GCC and vegetation
398 products derived from MERIS were varied. Weak relationships were demonstrated at some study sites
399 dominated by several juxtaposing land cover types such as Cary Institute of Ecosystem Studies, although
400 this was not universally the case. Others were characterised by strong relationships, reflecting the mixed
401 nature of the findings of Klosterman et al. (2014). The observed seasonal differences in the strength and
402 significance of these relationships are to be expected, as the degree of variation that can be explained by
403 the GCC is substantially reduced in the summer and winter, during which the condition of vegetation
404 remains relatively static.

405 An unexpected result of this study was the fact that weak relationships were demonstrated between the
406 GCC and MGCC, as the MGCC was calculated to provide a more direct spectral comparison to the near-
407 surface remote sensing data itself. Nevertheless, similar results were obtained by Klosterman et al. (2011),
408 who report that when calculated from MODIS data, the GCC is subject to a substantial degree of noise,
409 poorly representing seasonal patterns when compared to other vegetation products such as the Enhanced
410 Vegetation Index (EVI) and NDVI. The noise observed in the MGCC is likely due to the fact that unlike the
411 other vegetation products derived from MERIS, it incorporates a band at blue wavelengths (band 2,
412 centered at 442.5 nm). In the optical domain, it is these shorter wavelengths that are most strongly
413 influenced by atmospheric effects, a fact reflected by the greater degree of variation observed at all study
414 sites in band 2 when compared to band 13 (centered at 865 nm) (Figure 9). Because the MERIS L2 FRS
415 data are subject only to partial atmospheric correction, residual contamination of the blue band is more
416 likely.



417 Figure 9: Coefficient of variation associated with reflectance values in MERIS bands 2 and 13 (centered at 442.5 nm
 418 and 865 nm respectively) at each study site during the summer.
 419

420
 421 *4.3. Potential of near-surface remote sensing for evaluating satellite-derived vegetation products*

422 As discussed in Section 1.3, near-surface remote sensing has been adopted by the phenological research
 423 community as an alternative to in-situ observations of events such as bud-burst and leaf opening. It is a
 424 particularly promising technique for the evaluation of satellite-derived phenological transition dates,
 425 enabling the phenological characteristics of an entire canopy to be characterised as opposed to those of a
 426 single plant (Hufkens et al., 2012; Keenan et al., 2014; Klosterman et al., 2014). Additionally, as the same
 427 algorithms used to derive phenological transition dates from satellite-derived vegetation products can be
 428 applied to near-surface remote sensing data, their results can be more easily compared. Consistent with
 429 the results of previous studies, clear seasonal patterns in the GCC were observed at deciduous forest sites
 430 from which it would be straightforward to derive phenological transition dates. In light of the noise observed
 431 at evergreen forest and grassland sites, another foreseeable application of near-surface remote sensing
 432 data is the evaluation of cloud-screening algorithms. By analysing the DN values of an ROI covering the
 433 sky, it might be possible to automatically determine the presence or absence of cloud cover. This could
 434 provide particularly useful information in the case of instruments such as MERIS and OLCI, whose cloud-
 435 screening algorithms are constrained by the absence of bands at shortwave- and thermal-infrared
 436 wavelengths.

437 Despite the advantages of the technique, the results of this study reveal several issues associated with
438 near-surface remote sensing that limit its potential for the evaluation of the underlying satellite-derived
439 vegetation products. Our analysis indicates that the relationship between the GCC and vegetation products
440 derived from MERIS is in some cases distinctly non-linear, saturating asymptotically at medium to high
441 MGCC, MGVI, MTCI, and NDVI values. This is an important consideration for those attempting to model
442 variables related to plant function such as GPP, particularly in the case of study sites characterised by
443 medium to high biomass. Keenan et al. (2014) note a similar non-linear relationship between the GCC and
444 in-situ observations of LAI, suggesting that increases in the GCC occur as a result of green leaves filling
445 gaps within the canopy. Above an LAI of approximately 2.5, few gaps remain in the canopy, and because
446 additional leaves overlap one another, the greenness of the canopy, as observed by the digital camera,
447 does not increase (Keenan et al., 2014). We note that the majority of satellite-derived vegetation products
448 remain sensitive to increases in LAI, as a result of a) their near-nadir viewing geometry, and b) the fact that
449 they incorporate bands at near-infrared wavelengths, where the reflectance of leaves is governed more
450 strongly by structural characteristics as opposed to pigmentation. As such, the exploitation of near-infrared
451 capabilities, as demonstrated by Petach et al. (2014) and now available at 200 PhenoCam sites, would
452 likely enable the issue of asymptotic saturation to be at least partially overcome in future investigations.

453

454 **5. Conclusions**

455 Although near-surface remote sensing has been used to evaluate satellite-derived phenological transition
456 dates, few studies have considered shape and magnitude of the underlying time-series. In this study, for
457 the first time, we investigated the relationship between continuous measures of canopy greenness derived
458 using near-surface remote sensing and satellite-derived vegetation products. Temporal inconsistencies
459 were observed between the GCC and vegetation products derived from MERIS, reflecting the results of
460 previous work. Although temporal inconsistencies have previously been attributed to the oblique viewing
461 geometry of the digital cameras, they are also to be expected due to differences in the incorporated spectral
462 bands, which provide sensitivity to different biophysical variables. As in other studies, a spring peak and
463 summer decline were observed in the GCC at deciduous forest sites. Whilst the spring peak has previously
464 been attributed to the non-linear relationship between the leaf chlorophyll concentration and the GCC, the
465 results of our radiative transfer modelling suggest that seasonal variations in brown pigment concentration,
466 and to a lesser extent illumination geometry, contribute to the summer decline.

467 Moderate to strong relationships between the GCC and vegetation products derived from MERIS were
468 demonstrated at deciduous forest sites. Weak relationships were demonstrated at evergreen forest sites
469 as a result of their comparatively subtle seasonality, which is likely masked by atmospheric, BRDF, and
470 shadowing effects in the vegetation products derived from MERIS. At these sites, seasonal patterns were
471 better resolved by the GCC, highlighting the need for more rigorous atmospheric and BRDF correction
472 schemes.

473 As a result of its increased sensitivity to initial increases in canopy greenness when compared to the
474 vegetation products derived from MERIS, the GCC is particularly well-suited to identifying the start of
475 season, making near-surface remote sensing a valuable source of data for evaluating satellite-derived
476 phenological transition dates. Nevertheless, the results of this study reveal that in some cases, the
477 relationship between the GCC and vegetation products derived from MERIS saturates asymptotically at
478 medium to high MGCC, MGVI, MTCI, and NDVI values. At present, this limits the potential of the approach
479 for the evaluation of the underlying satellite-derived vegetation products, and for the continuous monitoring
480 of vegetation during the growing season, particularly at medium to high biomass study sites. Nevertheless,

481 if coupled with near-infrared capabilities, we suggest that near-surface remote sensing has the potential to
482 serve as a useful tool for the operational and systematic evaluation of satellite-derived vegetation products.

483 **Acknowledgements**

484 This work was supported by ESA and a University of Southampton Vice-Chancellor's Scholarship. The
485 authors thank the PhenoCam network for access to near-surface remote sensing data, Alessandro Burini
486 and the G-POD team for their assistance in MERIS data processing, and Jérôme Ogée for providing the
487 IDL routines used by Wingate et al. (2015) to simulate GCC values at Alice Holt Research Forest.

488 The development of PhenoCam has been supported by the Northeastern States Research Cooperative,
489 NSF's Macrosystems Biology program (award EF-1065029), DOE's Regional and Global Climate Modelling
490 program (award DE-SC0016011), and the US National Park Service Inventory and Monitoring Program and
491 the USA National Phenology Network (grant number G10AP00129 from the United States Geological
492 Survey). We acknowledge additional support, through the National Science Foundation's LTER program,
493 for research at Harvard Forest (DEB-1237491), and Bartlett Experimental Forest (DEB-1114804).

494 **References**

- 495 Baret, F., Hagolle, O., Geiger, B., Bicheron, P., Miras, B., Huc, M., Berthelot, B., Niño, F., Weiss, M.,
496 Samain, O., Roujean, J.L. and Leroy, M. 2007, LAI, fAPAR and fCover CYCLOPES global products derived
497 from VEGETATION: part 1: principles of the algorithm, *Remote Sens. Environ.*, vol. 110, no. 3, pp. 275-
498 286.
- 499 Baret, F., Weiss, M., Allard, D., Garrigue, S., Leroy, M., Jeanjean, H., Fernandes, R., Myneni, R., Privette,
500 J., Morisette, J., Bohbot, H., Bosseno, R., Dedieu, G., Di Bella, C., Duchemin, B., Espana, M., Gond, V.,
501 Gu, X.F., Guyson, D., Lelong, C., Maisongrande, P., Mougín, E., Nilson, T., Verousraete, F. and Vintilla, R.
502 2005, *VALERI: a network of sites and a methodology for the validation of medium spatial resolution land*
503 *satellite products*, IRNA, Avignon, France.
- 504 Barker, K., Mazeran, C., Lerebourg, C., Bouvet, M., Antoine, D., Ondrusek, M., Zibordi, G. and Lavender,
505 S. 2008, 'MERMAID: the MERIS matchup in-situ database', in *Proceedings of the 2nd MERIS/(A)ATSR*
506 *User Workshop*, September 2008, Frascati, Italy.
- 507 Barnes, W.L., Pagano, T.S. and Salomonson, V.V. 1998, Prelaunch characteristics of the Moderate
508 Resolution Imaging Spectroradiometer (MODIS) on EOS-AM1, *IEEE Trans. Geosci. Remote Sens.*, vol.
509 36, no. 4, pp. 1088-1100.
- 510 Baumann, M., Ozdogan, M., Richardson, A.D. and Radeloff, V.C. 2017, Phenology from Landsat when
511 data is scarce: using MODIS and dynamic time-warping to combine multi-year Landsat imagery to derive
512 annual phenology curves, *Int. J. Appl. Earth Obs. Geoinf.*, vol. 54, pp. 72-83.
- 513 Carlson, T.N. and Ripley, D.A. 1997, On the relation between NDVI, fractional vegetation cover, and leaf
514 area index, *Remote Sens. Environ.*, vol. 62, no. 3, pp. 241-252.
- 515 Chander, G., Mishra, N., Helder, D.L., Aaron, D.B., Angal, A., Choi, T., Xiong, X., and Doelling, D.R. 2013,
516 Applications of spectral band adjustment factors (SBAF) for cross-calibration, *IEEE Trans. Geosci. Remote*
517 *Sens.*, vol. 51, no. 3.

518 Coops, N.C., Hilker, T., Bater, C.W., Wulder, M.A., Nielsen, S.E., McDermid, G. and Stenhouse, G. 2012,
519 Linking ground-based to satellite-derived phenological metrics in support of habitat assessment, *Remote*
520 *Sens. Lett.*, vol. 3, no. 3, pp. 192-200.

521 Dash, J. and Curran, P.J. 2004, The MERIS terrestrial chlorophyll index, *Int. J. Remote Sens.*, vol. 25, no.
522 23, pp. 5403-5413.

523 Demarez, V., Gastellu-Etchegorry, J.P., Mougín, E., Marty, G., Proisy, C., Dufrêne, E. and le Dantec, V.
524 1999, Seasonal variation of leaf chlorophyll content of a temperate forest: inversion of the PROSPECT
525 model, *Int. J. Remote Sens.*, vol. 20, no. 5, pp. 879-894.

526 Donlon, C., Berruti, B., Buogiorno, A., Ferreira, M.H., Féménias, P., Frerick, J., Goryl, P., Klein, U., Laur,
527 H., Mavrocordatos, C., Nieke, J., Rebhan, H., Seitz, V., Stroede, J., Sciarra, R. 2012, The Global Monitoring
528 for Environment and Security (GMES) Sentinel-3 mission, *Remote Sens. Environ.*, vol. 120, pp. 37-57.

529 EC. 2005, *Global Monitoring for Environment and Security (GMES): From Concept to Reality*, European
530 Commission, Brussels.

531 ESA. 2006, *MERIS Products Quality Status Report: MEGS 7.4 and IPF 5*, European Space Agency,
532 Frascati, Italy.

533 ESA. 2012, *Sentinel-3: ESA's Global Land and Ocean Mission for GMES Operational Services*, European
534 Space Agency Communications, Noordwijk, Netherlands.

535 FAO, 2010. *Global Forest Resources Assessment 2010: Main Report*, Food and Agriculture Organisation
536 of the United Nations, Rome.

537 Feeny, P.P., and Bostock, H. 1968, Seasonal changes in the tanning content of oak leaves,
538 *Phytochemistry.*, vol. 7, no. 5, pp. 871-880.

539 Fernandes, R., Plummer, S. and Nightingale, J., Baret, F., Camacho, F., Fang, H., Garrigues, S., Gobron,
540 N., Lang, M., Lacaze, R., LeBlanc, S., Meroni, M., Martinez, B., Nilson, T., Pinty, B., Pisek, J., Sonnentag,
541 O., Verger, A., Welles, J., Weiss, M. and Widlowski, J.L. 2014, 'Global Leaf Area Index Product Validation
542 Good Practices', in Schaeppman-Strub, G., Román, M. and Nickeson, J. (eds) *Best Practice for Satellite-*

543 *Derived Land Product Validation*, Committee on Earth Observation Satellites Working Group on Calibration
544 and Validation, Greenbelt, Maryland, United States.

545 Foley, J.A., Ramankutty, N., Brauman, K.A., Cassidy, E.S., Gerber, J.S., Johnston, M., Mueller, N.D.,
546 O'Connell, C., Ray, D.K., West, P.C., Balzer, C., Bennet, E.M., Carpenter, S.R., Hill, J., Monfreda, C.,
547 Polasky, S., Rockström, J., Sheehan, J., Siebert, S., Tilman, D. and Zaks, D.P.M. 2011, Solutions for a
548 cultivated planet, *Nature*, vol. 478, no. 7369, pp. 337-342.

549 Gates, D.M., Keegan, H.J., Schleter, J.C. and Weidner, V.R. 1965, Spectral properties of plants, *Appl.*
550 *Opt.*, vol. 4, no. 1, pp. 11-20.

551 GCOS. 2012, *GCOS Essential Climate Variables* [online], Global Climate Observing System, available:
552 <http://www.wmo.int/pages/prog/gcos/index.php> [accessed 19/09/2016].

553 Gobron, N., Pinty, B., Verstraete, M. and Govaerts, Y. 1999, The MERIS Global Vegetation Index (MGVI):
554 description and preliminary application, *Int. J. Remote Sens.*, vol. 20, no. 9, pp. 1917-1927.

555 Godfray, C.H., Beddington, J.R., Crute, I.R., Haddad, L., Lawrence, D., Muir, J.F., Pretty, J., Robinson, S.,
556 Thomas, S.M. and Toulmin, C. 2010, Food security: the challenge of feeding 9 billion people, *Science*, vol.
557 327, no. 5967, pp. 812-818.

558 Gómez-Chova, L., Camps-Valls, G., Calpe-Maravilla, J., Gaunter, L. and Moreno, J. 2007, Cloud-screening
559 algorithms for ENVISAT/MERIS multispectral images, *IEEE Trans. Geosci. Remote Sens.*, vol. 45, no. 12,
560 pp. 4105-4118.

561 Gond, V., de Pury, D.G.G., Veroustraete, F. and Ceulemans, R. 1999, Seasonal variations in leaf area
562 index, leaf chlorophyll, and water content; scaling-up to estimate fAPAR and carbon balance in a multilayer,
563 multispecies forest, *Tree Physiol.*, vol 19, pp. 673-679.

564 Homer, C.G., Dewitz, J.A., Yang, L., Jin, S., Danielson, P., Xian, G., Coulston, J., Herold, N.D., Wickham,
565 J.D., and Megown, K. 2015, Completion of the 2011 National Land Cover Database for the conterminous
566 United States – representing a decade of land cover change information, *Photogramm. Eng. Remote Sens.*,
567 vol. 81, no. 5, pp. 345-354.

568 Hufkens, K., Friedl, M., Sonnentag, O., Braswell, B.H., Milliman, T. and Richardson, A.D. 2012, Linking
569 near-surface and satellite remote sensing measurements of deciduous broadleaf forest phenology, *Remote*
570 *Sens. Environ.*, vol. 117, pp. 307-321.

571 Ide, R. and Oguma, H. 2010, Use of digital cameras for phenological observations, *Ecol. Inform.*, vol. 10,
572 pp. 1689-1706.

573 Jacquemoud, S. and Baret, F. 1990, PROSPECT: a model of leaf optical properties spectra, *Remote Sens.*
574 *Environ.*, vol. 34, pp. 75-91.

575 Jacquemoud, S., Verhoef, W., Baret, F., Bacour, C., Zarco-Tejada, P.J., Asner, G.P., François, C. and
576 Ustin, S.L. 2009, PROSPECT + SAIL models: a review of use for vegetation characterization, *Remote*
577 *Sens. Environ.*, vol. 113, pp. S56-S66.

578 Justice, C., Belwards, A., Morisette, J., Lewis, P., Privette, J. and Baret, F. 2000, Developments in the
579 'validation' of satellite sensor products for the study of the land surface, *Int. J. Remote Sens.*, vol. 21, no.
580 17, pp. 3383-3390.

581 Justice, C.O., Román, M.O., Csiszar, I., Vermote, E.F., Wolfe, R.E., Hook, S.J., Friedl, M., Wang, Z.,
582 Schaaf, C.B., Mirua, T., Tschudi, M., Riggs, G., Hall, D.K., Lyapustin, A.I., Devadiga, S., Davidson, C. and
583 Masuoka, E.J. 2013, Land and cryosphere products from NPP VIIRS: overview and status, *J. Geophys.*
584 *Res. Atmos.*, vol. 118, no. 17, pp. 9753-9765.

585 Keenan, T.F., Darby, B., Felts, E., Sonnentag, O., Fridel, M.A., Hufkens, K., O'Keefe, J., Klosterman, S.,
586 Munger, J.W., Toomey, M. and Richardson, A.D. 2014, Tracking forest phenology and season physiology
587 using digital repeat photography: a critical assessment, *Ecol. Appl.*, vol. 24, no. 6, pp. 1478-1489.

588 Klosterman, S.T., Hufkens, K., Gray, J.M., Melaas, E., Sonnentag, O., Lavine, I., Mitchell, L., Norman, R.,
589 Friedl, M.A. and Richardson, A.D. 2014, Evaluating remote sensing of deciduous forest phenology at
590 multiple spatial scales using PhenoCam imagery, *Biogeosciences*, vol. 11, pp. 4305-4320.

591 Knyazikhin, Y., Glassy, J., Privette, J.L., Tian, Y., Lotsch, A., Zhang, Y., Wang, Y., Morisette, J.T., Votava,
592 P., Myneni, R.B., Nemani, R.R. and Running, S.W. 1999, *MODIS Leaf Area Index (LAI) and Fraction of*

593 *Photosynthetically Active Radiation Absorbed by Vegetation (FPAR) Product (MOD15) Algorithm*
594 *Theoretical Basis Document*, Boston University, Boston, United States.

595 Koike, T. 1990, Autumn coloring, photosynthetic performance and leaf development of deciduous broad-
596 leaved trees in relation to forest succession, *Tree Physiol.*, vol 7, pp. 21-32.

597 Lichenthaler, H.K., Wenzel, O., Buschmann, C. and Gitelson, A. 1998, Plant stress detection by reflectance
598 and fluorescence, *Ann. N.Y. Acad. Sci.*, vol. 851, pp. 271-285.

599 Liu, Y, Hill, M.J., Zhang, M., Wang, Z., Richardson, A.D., Hufkens, K., Filippa, G., Baldocchi, D.D., Ma, S.,
600 Verfaillie, J. and Schaaf, C.B. 2017, Using data from Landsat, MODIS, VIIRS and PhenoCams to monitor
601 the phenology of California oak/grass savanna and open grassland across spatial scales, *Agric. For.*
602 *Meteorol.*, vol. 237-238, pp. 311-325

603 Maisongrande, P., Duchemin, B. and Dedieu, G. 2004, VEGETATION/SPOT: an operational mission for
604 the Earth monitoring; presentation of new standard products, *Int. J. Remote Sens.*, vol. 25, no. 1, pp. 9-14.

605 Mélin, F., Zibordi, G., Berthon, J., Bailey, S., Franz, B., Voss, K., Flora, S. and Grant, M. 2011, Assessment
606 of MERIS reflectance data as processing with SeaDAS over the European seas, *Opt. Express*, vol. 19, no.
607 25, pp. 25657-25671.

608 Migliavacca, M., Galvagno, M., Cremonese, E., Rossini, M., Meroni, M., Sonnentag, O., Cogliati, S., Manc,
609 G., Diotri, F., Busetto, L., Cescatti, A., Colombo, R., Fava, F., Morra di Cella, U., Pari, E., Siniscalco, C. and
610 Richardson, A.D. 2011, Using digital repeat photography and eddy covariance data to model grassland
611 phenology and photosynthetic CO₂ uptake, *Agric. For. Meteorol.*, vol. 151, no. 10, pp. 1325-1337.

612 Morisette, J.T., Baret, F., Privette, J., Myneni, R.B., Nickeson, J.E., Garrigues, S., Shabanov, N.V., Weiss,
613 M., Fernandes, R.A., Leblanc, S.G., Kalacska, M., Sánchez-Azofeifa, G.A., Chubey, M., Rivard, B.,
614 Stenberg, P., Rautiainen, M., Voipio, P., Manninen, T., Pilant, A.N., Lewis, T.E., Iiames, J.S., Colombo, R.,
615 Meroni, M., Busetto, L., Cohen, W.B., Turner, D.P., Warner, E.D., Petersen, G.W., Seufert, G. and Cook,
616 R. 2006, Validation of global moderate-resolution LAI products: a framework proposed within the CEOS
617 land product validation subgroup, *IEEE Trans. Geosci. Remote Sens.*, vol. 44, no. 7, pp. 1804-1817.

618 Morisette, J.T., Privette, J.L. and Justice, C.O. 2002, A framework for the validation of MODIS land
619 products, *Remote Sens. Environ.*, vol. 83, no. 1, pp. 77-96.

620 Morra di Cella, U., Bocca, M., Busetto, L., Colombo, R., Cremonese, E., Delestrade, A., Galvagno, M.,
621 Loison, A., Lopez, J.F., Meroni, M., Migliavacca, M., Tutino, S. and Yoccoz, N.G. 2009, 'PHENOALP: a
622 new project on phenology in the Western Alps', in *Proceedings of the 4th Symposium of the Hohe Tauern
623 National Park for Research in Protected Areas*, September 2009, Kaprun, Salzburg, Austria.

624 Myneni, R.B. and Williams, D.L. 1994, On the relationship between FAPAR and NDVI, *Remote Sens.
625 Environ.*, vol. 49, no. 3, pp. 200-211.

626 Myneni, R.B., Hoffman, S., Knyazikhim, Y., Privette, J.L., Glassy, J., Tian, Y., Wang, Y., Song, X., Zhang,
627 Y., Smith, G.R., Lotsch, A., Friedl, M., Morisette, J.T., Votava, P., Nemani, R.R. and Running, S.W. 2002,
628 Global products of vegetation leaf area and fraction absorbed PAR from year one of MODIS data, *Remote
629 Sens. Environ.*, vol. 83, no. 1, pp. 214-231.

630 Nijland, W., Bolton, D.K., Coops, N.C. and Stenhouse, G. 2016, Imaging phenology: scaling from camera
631 plots to landscapes, *Remote Sens. Environ.*, vol. 177, pp. 13-20.

632 Petach, A.R., Toomey, M., Aubrecht, D.M. and Richardson, A.D. 2014, Monitoring vegetation phenology
633 using an infrared-enabled security camera, *Agric. For. Meteorol.*, vol. 195-196, pp. 143-151

634 QA4EO. 2010, *Quality Assurance Framework for Earth Observation* [online], available: <http://qa4eo.org/>
635 [accessed 19/09/2016].

636 Rast, M., Bézy, J.L. and Bruzzi, S. 1999, The ESA Medium Resolution Imaging Spectrometer (MERIS): a
637 review of the instrument and its mission, *Int. J. Remote Sens.*, vol. 20, no. 9, pp. 1681-1702.

638 Richardson, A.D., Braswell, B.H., Hollinger, D.Y., Jenkins, J.P. and Ollinger, S.V. 2009, Near-surface
639 remote sensing of spatial and temporal variation in canopy phenology, *Ecol. Appl.*, vol. 19, no. 6, pp. 1417-
640 1428.

641 Richardson, A.D., Duigan, S.P. and Berlyn, G.P. 2002, An evaluation of noninvasive methods to estimate
642 foliar chlorophyll content, *New Phytol.*, vol. 153, pp. 185-194.

643 Richardson, A.D., Jenkins, J.P., Braswell, B.H., Hollinger, D.Y., Ollinger, S.V. and Smith, M. 2007, Use of
644 digital webcam images to track spring green-up in a deciduous broadleaf forest, *Oecologia*, vol. 152, no. 2,
645 pp. 323-334.

646 Rouse, J.W., Haas, R.H., Schell, J.A. and Deering, D.W. 1973, 'Monitoring vegetation systems in the Great
647 Plains with ERTS', in *Proceedings of the Third Earth Resources Technology Satellite-1 Symposium*,
648 December 1973, Goddard Space Flight Centre, Washington D.C., United States.

649 Sá, C., D'Alimonte, D., Brito, A.C., Kajiyama, T., Mendes, C.R., Vitorino, J., Oliveira, P.B., da Silva, J.C.B.
650 and Brotas, V. 2015, Validation of standard and alternative satellite ocean-colour chlorophyll products off
651 Western Iberia, *Remote Sens. Environ.*, vol. 168, pp. 403-419.

652 Santer, R., Carrere, V., Dubuisson, P. and Roger, J.C. 1999, Atmospheric correction over land for MERIS,
653 *Int. J. Remote Sens.*, vol. 20, no. 9, pp. 1819-1840.

654 Sellers, P.J., Dickinson, R.E., Randall, D.A., Betts, A.K., Hall, F.G., Berry, J.A., Collatz, G.J., Denning, A.S.,
655 Mooney, H.A., Nobre, C.A., Sato, N., Field, C.B., Henderson-Sellers, A. 1997, Modelling the exchanges of
656 energy, water, and carbon between continents and the atmosphere, *Science*, vol. 275, no. 5299, pp. 502-
657 509.

658 Sonnentag, O., Hufkens, K., Teshera-Sterne, C., Young, A.M., Friedl, M., Braswell, B.H., Milliman, T.,
659 O'Keefe, J. and Richardson, A.D. 2012, Digital repeat photography for phenological research in forest
660 ecosystems, *Agric. For. Meteorol.*, vol. 152, pp. 159-177.

661 Toomey, M., Friedl, M.A., Frohking, S., Hufkens, K., Klosterman, S., Sonnentag, O., Baldocchi, D.D.,
662 Bernacchi, C.J., Biraud, S.C., Bohrer, G., Brzostek, E., Burns, S.P., Coursolle, C., Hollinger, D.Y., Margolis,
663 H.A., McCaughey, H., Monson, R.K., Munger, J.W., Pallardy, S., Phillips, R.P., Torn, M.S., Wharton, S.,
664 Zeri, M. and Richardson, A.D. 2015, Greenness indices from digital cameras predict the timing and
665 seasonal dynamics of canopy-scale photosynthesis, *Ecol. Appl.*, vol. 25, no. 1, pp. 99-115.

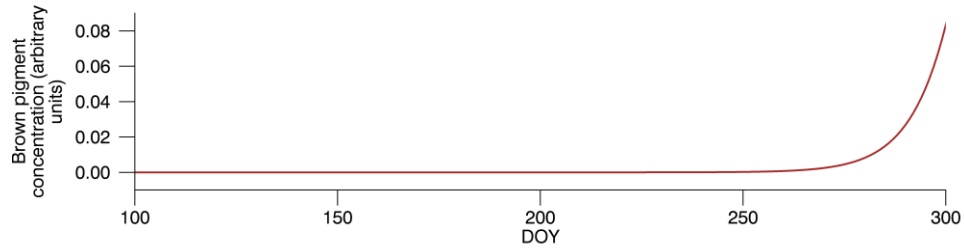
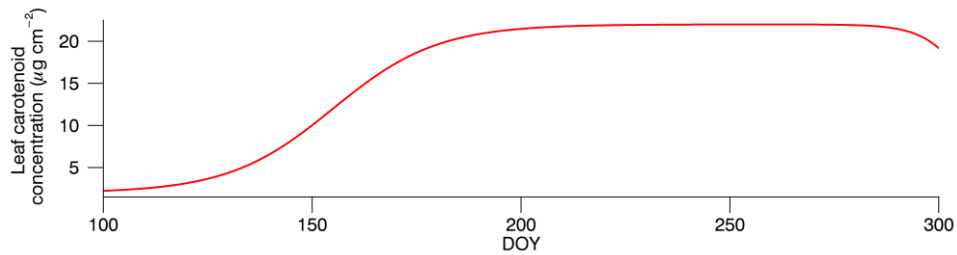
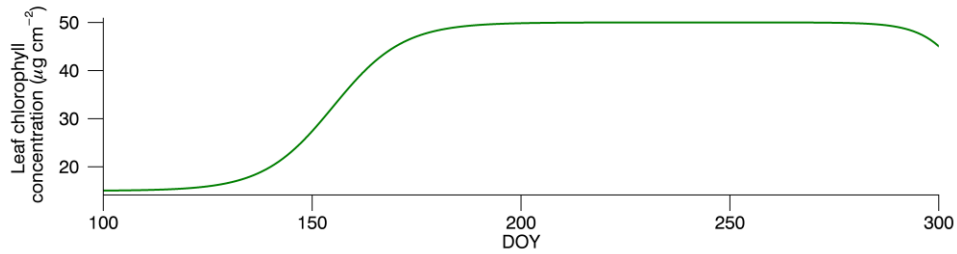
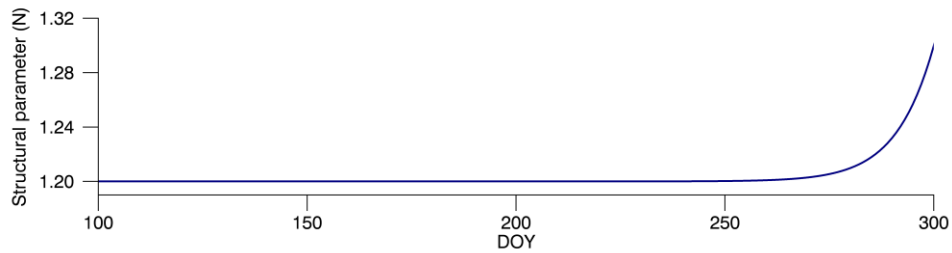
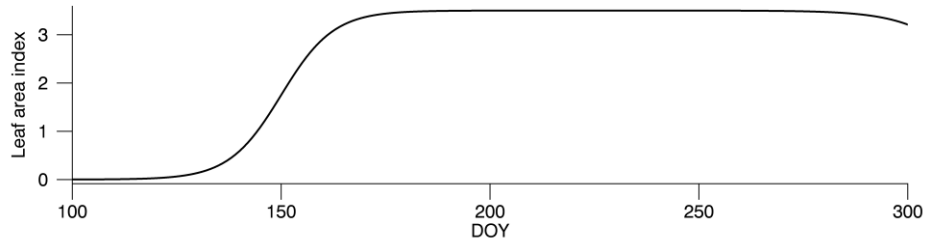
666 Verhoef, W. 1984, Light scattering by leaf layers with application to canopy reflectance modelling: the SAIL
667 model, *Remote Sens. Environ.*, vol 16, pp. 125-141.

668 Wingate, L., Ogée, J., Cremonese, E., Filippa, G., Mizunuma, T., Migliavacca, M., Moisy, C., Wilkinson, M.,
669 Moureaux, C., Wohlfahrt, G., Hammerle, A., Hörtnagl, L., Gimeno, C., Porcar-Castell, A., Galvagno, M.,
670 Nakaji, T., Morison, J., Kolle, O., Knohl, A., Kutsch, W., Kolari, P., Nikinmaa, E., Ibrom, A., Gielen, B.,
671 Eugster, W., Balzarolo, M., Papale, D., Klumpp, K., Köstner, B., Gründwald, T., Joffre, R., Ourcival, J.M.,
672 Hellstrom, M., Lindroth, A., Charles, G., Longdoz, B., Genty, B., Levula, J., Heinsch, B., Sprintsin, M., Yakir,
673 D., Manise, T., Guyon, D., Ahrends, H., Plaza-Aguilar, A., Gaun, J.H. and Grace, J. 2015, Interpreting
674 canopy development and physiology using the EUROPHEN camera network at flux sites, *Biogeosciences*,
675 vol. 12, pp. 7979-8034.

676 Yang, X., Tang, J. and Mustard, J.F. 2014, Beyond leaf colour: comparing camera-based phenological
677 metrics with leaf biochemical, biophysical and spectral properties throughout the growing season of a
678 temperate deciduous forest, *J. Geophys. Res. Biogeosci.*, vol. 119., no. 3, pp. 181-191.

679 **Appendix A**

680



685

686

687

688

Figure A.1: Varying PROSPECT and SAIL parameters used to simulate GCC values over the course of the spring and summer at Alice Holt Research Forest, after Wingate et al. (2015). Brown pigment concentration values were rescaled to the range 0 to 1.

689 Table A.1: Constant PROSPECT and SAIL parameters used to simulate GCC values over the course of the spring
 690 and summer at Alice Holt Research Forest, after Wingate et al. (2015).

Parameter	Value
Hot spot parameter	0.05
Average leaf angle (°)	30
Observer zenith angle (°)	80
Relative azimuth angle (°)	0
Diffuse to direct radiation (%)	25
Soil coefficient	0.2
Water thickness (cm)	0.04
Dry matter (g cm ⁻²)	0.008

691

692 Table A.2: Details of the wavelengths averaged to approximate the red, green and blue bands of a digital camera
 693 from PROSPECT and SAIL output spectra.

Band	Wavelength (nm)		
	Minimum	Centre	Maximum
Blue	400	450	500
Green	500	550	600
Red	600	650	700

694

695 **Appendix B**

696

697 Table B.1: Spearman's rank correlation coefficient (r_s) values associated with each satellite-derived vegetation product at each study site, by season. Values
 698 marked with * indicate that the relationship with the GCC was statistically significant ($p < 0.01$).

Site	Spearman's rank correlation coefficient															
	Spring				Summer				Autumn				Winter			
	MGCC	MGVI	MTCI	NDVI	MGCC	MGVI	MTCI	NDVI	MGCC	MGVI	MTCI	NDVI	MGCC	MGVI	MTCI	NDVI
Arbutus Lake	0.66*	0.44	-0.47	0.56	0.07	0.48	0.61	0.25	0.49	0.59*	0.63*	0.69*	0.37	0.01	-0.12	-0.11
Bartlett Experimental Forest (IR)	0.29	0.50*	-0.04	0.28	-0.21	0.22	0.07	-0.07	0.25	0.87*	0.66*	0.26	0.22	0.14	0.01	0.07
Cary Institute of Ecosystem Studies	0.47*	0.81*	0.70*	0.67*	0.22	0.01	0.06	0.06	0.25	0.51	0.57*	0.24	-0.12	-0.17	0.46	0.09
Coweeta Hydrologic Laboratory	0.33	0.77*	0.73*	0.81*	-0.11	0.28	0.27	0.29	0.25	0.68*	0.91*	0.77*	0.23	0.42	-0.03	0.18
Harvard Forest	0.62*	0.61*	0.23	0.58*	-0.01	0.00	-0.32	0.09	0.49*	0.71*	0.80*	0.74*	0.16	-0.30	-0.06	-0.33
Harvard Forest Hemlock	0.44	0.33	0.23	0.27	-0.11	0.07	-0.23	0.08	0.30	0.65*	0.66*	0.68*	0.11	-0.15	0.03	-0.12
Little Prospect Hill	0.47	0.64*	0.03	0.61	0.19	0.24	-0.04	0.25	0.52*	0.80*	0.87*	0.83*	-0.23	0.16	0.10	0.20
Howland Experimental Forest	0.67*	0.33	-0.38	0.26	0.14	0.05	-0.34	0.07	0.16	0.59*	0.35	0.55*	0.51*	0.18	-0.16	0.25
Hubbard Brook Experimental Forest	0.33	0.49	-0.16	0.06	0.14	-0.11	-0.05	0.24	0.43	0.34	0.22	0.19	0.13	-0.25	-0.09	-0.08
Morgan Monroe State Forest	0.42*	0.76*	0.49*	0.48*	-0.04	0.15	0.11	-0.16	0.44*	0.72*	0.88*	0.52*	0.29	0.00	0.63*	-0.03
Proctor Maple Research Center	0.63*	0.87*	0.41	0.84*	-0.20	-0.14	-0.35	-0.08	0.57*	0.73*	0.79*	0.83*	-0.05	0.22	-0.25	0.30
University of Michigan Biological Station	0.66	0.90*	-0.24	0.90*	0.01	0.04	0.45	0.22	0.64	0.85*	0.81*	0.93*	-	-	-	-
Vaira Ranch	0.04	0.38	0.04	0.23	-0.39*	-0.57*	0.23*	-0.60*	-0.65*	-0.84*	0.71*	-0.86*	0.43	-0.49	-0.07	-0.34
Wind River Experimental Forest	-0.01	0.00	-0.09	-0.13	-0.21	-0.05	-0.23	-0.04	0.04	0.48*	0.12	0.50	-0.12	0.11	-0.17	0.07

699